Jefore Ethiopian Journal of Applied Sciences

ISSN 3006-6263 Volume 2(1), 2025

Journal homepage: www.jejas.org

Research Paper

Tuning Optical Properties of Cylindrical Nanoinclusions: The Roles of Metal Fraction, Passive and Active Host Matrices

Shewa Getachew Mamo

Department of Physics, Wolkite University, Wolkite, Ethiopia

Article History:

Received: 23 January 2025

Accepted: 08 December 2025

Published online: 29 December 2025

Keywords:

Plasmonics, Cylindrical Nanoinclusions, Quasistatic Approximation, Metal Fraction, Local Field Enhancement, Optical Bistability, Active Host Matrix

Abstract

The optical behavior of nanostructures is profoundly influenced by their geometry and the properties of the surrounding medium. While spherical nanoparticles have been extensively studied, cylindrical nanoinclusions offer unique anisotropic properties that are advantageous for integrated photonic devices. This work provides a comprehensive theoretical and numerical investigation into tuning the optical properties of cylindrical core-shell nanoinclusions, with a specific focus on the roles of metal fraction and the dielectric nature of passive versus active host matrices. By solving the Laplace equation within the quasistatic approximation (QA), we analyze the local field enhancement (LFE) and optical bistability (OB) for three distinct configurations: metal-coated dielectric cylinders (McDCs), dielectric-coated metal cylinders (DcMCs), and pure metal cylinders. A key finding is that these geometries exhibit fundamentally different resonant behaviors, from dual peaks in metal-coated systems to single peaks in the others. We demonstrate that the metal fraction p is a critical geometric parameter that controls the spectral position and strength of these resonances. Furthermore, the host matrix's dielectric function, particularly its imaginary part ε_h'', serves as a powerful material-based tuning knob. Active host matrices with a negative ε_h'' dramatically amplify the local field and modify OB characteristics by compensating for plasmonic losses. These insights establish clear design principles for optimizing cylindrical nanocomposites for advanced applications in nonlinear optics, all-optical switching, and high-sensitivity nanoscale sensing.

1. Introduction

Nanoparticles continue to attract significant scientific interest due to their unique optical properties, which diverge markedly from those of bulk materials (Zhang et al., 2022; Mamo, 2025). Among these, metal-dielectric nanostructures are particularly intriguing because their optical response is dominated by surface plasmon resonances (SPRs), collective oscillations of conduction electrons at the interfaces (Amendola & Pilot, 2021; Mamo, 2025). The ability to confine and enhance local electromagnetic fields at the nanoscale makes these systems fundamental to the field of plasmonics, with applications ranging from enhanced spectroscopy to nonlinear optics (Li et al., 2023; Lee et al., 2021; Mamo, 2025).

Author email: shewa.getachew@wku.edu.et

DOI: https://doi.org/10.70984/27rf4e73

Innovative methods of adjusting plasmonic characteristics include the application of core-shell (CS) topologies. Much research has been done on studying the optical characteristics of CS nanoparticles (i.e., extinction spectra, scattering cross-sections, and near-field enhancement) with regard to spherical type shape (Ali, 2024; Pirahlace et al., 2023; Mamo, 2025). More recently, complex structures like spheroidal and dimer shapes have been studied, showing how resonant behavior and light-matter interaction depend on both the physical shape and hybridization (Hitilli et al., 2024; Bergaga et al., 2023; Mamo, 2025). One of the most significant effects seen in nonlinear plasmonics is optical bistability (OB), where two stable output states can be reached by only one input intensity level. OB is extremely important for developing future optical memories and switches (Volz et al., 2021; Zhang & Wang, 2022; Mamo, 2025). Another important contributor to the strong nonlinear reactions (OB), which are evident in composite structures, is the significant local field enhancement generated by surface plasmon resonance (SPR) (Nugroho et al., 2022; Mamo, 2025).

Although the optical properties of spherical and spheroidal CS nanoparticles have been extensively studied, cylindrical-shaped geometries have been relatively less focused. This gap is of importance as cylindrical nanostructures (i.e., nanowires and rods) are becoming more and more interesting for integrated photonic circuits and sensing platforms, thanks to their anisotropic behavior and larger field enhancement factors (Kumar & Singh, 2023; Chen et al., 2021). Additionally, the importance of the host matrix is rather underestimated. Many works consider a passive lossless dielectric background. However, an active host matrix with a negative imaginary part of its dielectric function can provide optical gain, compensating for metallic losses and dramatically altering the plasmonic response (Li et al., 2021; Wang et al., 2023). The interplay between the gain provided by an active host and the unique field distribution around cylindrical nanoinclusions remains a nascent area of research.

In the past few years, new literature has emerged that looks more closely at how the geometric structure and gain of particles can yield enhanced optical performance than previously understood. Movsisyan and Parsanyan (2024) investigated the enhanced optical brightness of plasmonic core-shell dimers, in which they demonstrated that nanostructure geometry can significantly affect non-linear optical properties. Hirpha et al. (2024) have investigated the non-linear optical breins functioning in composite spheroidal core-shell nanostructure systems with an active dielectric core and also discovered significant gain achieved through the geometrical differences between core-shell nanostructured composites with various characteristics. Neither of these studies demonstrates a systematic study on the influence of dielectric materials on light field enhancement and optical brightness in cylindrical core-shell nano-inclusions.

The proposed research endeavors to fill this gap by offering a theoretical and numerical study. The primary aim of this research is to discuss and reveal the local field enhancement and bistability effects within a cylinder-shaped nanoinclusion, especially for three different setups: MDCDs, DMCs, and metallic cylinders. Based on the QA approach, this research will describe the local field enhancement factor and its sensitivity to the metallic component and both the real and imaginary parts of the dielectric constant of the host materials. Based on the approach provided within this research, and by comparing the performances within both passive and active host matrices, this research is essential for designing and optimizing cylinder-shaped nanocomposites for novel nanophtonic device applications.

2. Simulations and theoretical basis

By using the quasistatic technique, we used theoretical and numerical analysis to investigate the OB and LFE properties of the nanocomposites. Our research was centered on cylindrical CS NIs, in which the dielectric material with radius r_1 and dielectric function ε_h

is used to form the core. In contrast, the shell has a radius of r_2, and ε_m, the applied electric field, determines its dielectric function (DF). The entire nanocomposite is exposed to incidental electromagnetic radiation while implanted in a dielectric host matrix with a DF of ε_h. We took into consideration two options for the host matrix's DF to investigate the impact on the increasing local field and optical bistability. A material response to an applied electric field can determine whether the DF, represented by the symbol ε_h, is passive or active. The formula for this DF is (Rothwell et al., 2016; Getachew, 2024):

$$\varepsilon_h = \varepsilon_h' + i\varepsilon_h'' \quad (1)$$

ε_h' and ε_h'' represent the real and imaginary components of the DF of the host matrix material, respectively. The DF of the host matrix is regarded as passive when ε_h'' equals zero. Conversely, the dielectric function of the host matrix is deemed active when ε_h'' is smaller than zero. In order to evaluate each dielectric function's unique effects, we looked at both of its components independently in this study.

2.1. Distribution of electric potential in cylindrical core-shell nanoinclusions

To simulate the optical response in the case of cylindrical core-shell nano-inclusions (NIs) in an external electric field, we used the quasistatic approach. The quasistatic approach is applicable when the dimensions of the nano-inclusion are sufficiently smaller than the wavelength of the incoming light. Using the quasistatic approach, we can consider the problem to be an electrostatic problem. In fact, Laplace's equation for the electric potential can be used to address the issue. It turns out that the quasistatic approach is quite an effective analytical tool for analyzing local field enhancement. The system under consideration, illustrated schematically in Figure 1, consists of a cylindrical dielectric core with radius r_1 and dielectric function ε_d, surrounded by a metallic shell with an outer radius r_2 ($r_1 < r_2$) and dielectric function ε_m. This core-shell structure is embedded in a host medium characterized by a dielectric function ε_h. A uniform external electric field $\mathbf{E}_h = E_h \hat{z}$ is applied along the axis of the cylinder.

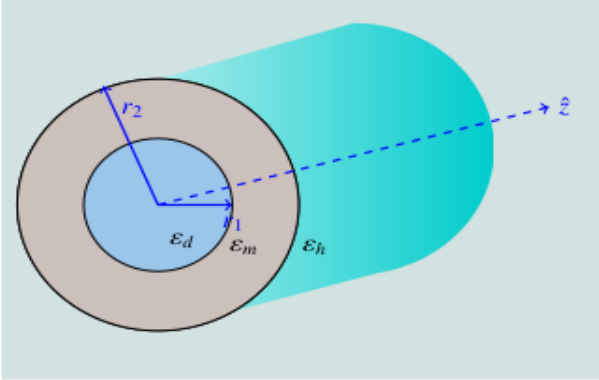

Figure 1. *Schematic of cylindrical nanoinclusions consisting of a dielectric core (radius r_1, dielectric constant ε_d) coated by a metallic shell (outer radius r_2, dielectric function ε_m), embedded in a host matrix (dielectric constant ε_h).*

The electric potential distribution within the dielectric core, metallic shell, and host matrix can be described by three separate functions: Φ_d for the DC, Φ_m for the metallic shell, and Φ_h for the host matrix. These functions are derived according to the equation provided in reference (Getachew, 2024; Buryi et al., 2011).

$$\Phi_d = -E_h Arcos\theta, r \leq r_1 \quad (2)$$

$$\Phi_m = -E_h\left(Br - \frac{C}{r}\right)cos\theta, r_1 \le r \le r_2 \quad (3)$$

$$\Phi_h = -E_h\left(r - \frac{D}{r}\right)cos\theta, r > r_2 \quad (4)$$

Here, the applied electric field is denoted by E_h, and the cylindrical coordinates of the observation point are denoted by r and θ. The vector E_h is aligned with the z-axis. The values of the coefficients A, B, C, and D are not provided and must be determined using the continuity equations for the displacement vector and electric potential at the interfaces between the shell-host matrix and *CS* boundaries. The electric potential is continuous at the interface of a core-shell nanocomposite between the dielectric core and the metallic shell. This notion is based on the idea that the electric potential across the interface cannot change abruptly; therefore, the potential values in the dielectric (core) and metallic (shell) regions must be equal at the interface. This condition can be expressed as:

$$\Phi_d = \Phi_m, r = r_1 \quad (5)$$

$$\Phi_m = \Phi_h, r = r_2 \quad (6)$$

The continuity of the displacement vector (which is related to the electric field) must also be maintained at the interface. This condition can be expressed as:

$$\varepsilon_d \frac{\partial \phi_d}{\partial r} = \varepsilon_m \frac{\partial \phi_m}{\partial r}, r = r_1 \quad (7)$$

$$\varepsilon_m \frac{\partial \phi_m}{\partial r} = \varepsilon_h \frac{\partial \phi_h}{\partial r}, r = r_2 \quad (8)$$

The dielectric constants of the dielectric core, metal shell, and dielectric host are represented by ε_d, ε_m, and ε_h, respectively. By solving equations 5, 6, 7, and 8 simultaneously, the values of the unknown coefficients can be determined as listed below.

$$A = \frac{4\varepsilon_m\varepsilon_h}{p\eta} \quad (9)$$

$$B = \frac{\varepsilon_h(\varepsilon_d + 2\varepsilon_m)}{p\eta} \quad (10)$$

$$C = \frac{2(\varepsilon_d - \varepsilon_m)}{p\eta} {r_1}^2 \quad (11)$$

$$D = \left(1 - 2\varepsilon_h \frac{(2-p)+\varepsilon_d p}{p\eta}\right) {r_2}^2 \quad (12)$$

Where, $p = 1 - \left(\frac{r_1}{r_2}\right)^2$ is the metal volume fraction in the inclusion,

$$\eta = {\varepsilon_m}^2 + \prod \varepsilon_m + \varepsilon_d\varepsilon_h \quad (13)$$

$$\prod = \left(\frac{2}{p} - 1\right)\varepsilon_d + \left(\frac{2}{p} - 1\right)\varepsilon_h \quad (14)$$

The Drude-Sommerfeld model is a theoretical framework used to describe the behavior of electrons in a metal, providing a simplified yet effective way to understand the electrical and optical properties of metals. This model offers a straightforward expression for the DF of the metal (ε_m). The dielectric function represents the material's response to an external electric field and determines its optical properties. From the Drude-Sommerfeld model, the *DF* of the metal (ε_m) is given by (Getachew & Berga, 2024):

$$\varepsilon_m = \varepsilon_\infty - \frac{1}{z(z+i\gamma)} \quad (15)$$

In this context, ε_∞ denotes the effect of bound electrons on polarizability. The variable z represents the ratio of the incident radiation frequency (ω) to the frequency of the bulk plasmon (ω_p), while γ indicates the ratio of the electron damping constant (ν) to the plasma frequency (ω_p). Additionally, the real and imaginary components of ε_m can be expressed as

$$\varepsilon_m = \varepsilon'_m + i\varepsilon''_m \quad (16)$$

Let's denote the parts, both real and imaginary of the equations above as follows:

$$\varepsilon'_m = \varepsilon'_\infty - \frac{1}{z(z+\gamma)}; \quad \varepsilon''_m = \varepsilon''_\infty + \frac{1}{z(z^2+\gamma z)}$$

2.2. Enhancing the local field of cylindrical NIs

The local field enhancement is a cornerstone of plasmonics, as the amplified field within or near a nanostructure drives nonlinear optical effects and enhances light-matter interactions. Within the quasistatic framework, the uniform applied field $\mathbf{E}_h = E_h\,\hat{z}$ induces a polarization in the nanoinclusion. The local electric field E local inside the nanostructure can be significantly different from, and often much stronger than, the applied field. For the cylindrical core-shell

geometry, the local field inside the dielectric core is of primary interest. As derived in Section 2.1, the potential inside the core is $\Phi_d = -E_h Arcos\theta$. The local electric field is obtained by taking the negative gradient of this potential:

$$E_{local} = -\nabla\Phi_d = AE_h\hat{z} \quad (17)$$

The complex coefficient A, which was determined by applying the electrostatic boundary conditions, is thus identified as the local field enhancement factor. Its magnitude squared, $|A|^2$, quantifies the enhancement of the electric field intensity within the core relative to the incident field intensity. This factor encapsulates the collective influence of the geometry (through the metal fraction p) and the dielectric properties of the core, shell, and host matrix. The following subsections present the derived expressions for $|A|^2$ for three fundamental configurations of cylindrical nanoinclusions, highlighting how the specific arrangement of materials dictates the plasmonic response and the resulting field enhancement.

2.2.1. Metal-covered dielectric cylindrical NIs

The ELF in the DC is obtained by substituting equation (16) into equation (9), and then squaring and simplifying the resulting expression.

$$|A|^2 = 16\frac{\left[\left(\varepsilon'_m\varepsilon'_h-\varepsilon''_m\varepsilon''_h\right)^2+\left(\varepsilon'_m\varepsilon''_h+\varepsilon''_m\varepsilon'_h\right)^2\right]}{p\left[\left(\varepsilon'_m+q'\varepsilon'_m-q''\varepsilon''_m+\varepsilon_d\varepsilon'_h\right)^2+\left(2\varepsilon_d\varepsilon''_m+q'\varepsilon''_m+q''\varepsilon'_m+\varepsilon_d\varepsilon''_h\right)^2\right]} \quad (18)$$

Where,

$$\varepsilon_h = \varepsilon'_h + i\varepsilon''_h, q = q' + iq''$$

$$q' = \left(\frac{2}{p}-1\right)(\varepsilon_d+\varepsilon'_h), q'' = -\left(\frac{2}{p}-1\right)\varepsilon''_h$$

2.2.2. Dielectric-covered metal cylindrical NIs

In the case of dielectric-coated metal cylindrical *NIs*, we can obtain the modified expression for the *LFE* by making a specific change to Eq. (9). This change involves replacing the dielectric constant ε_d with the dielectric constant of the metal ε_m, and replacing ε_m with ε_d in the equation. By doing so, we can derive the expression relevant to dielectric-coated metal cylindrical *NIs*. Consider the *CS* nanoinclusions, which consist of a dielectric core with a radius r_1 and dielectric permittivity ε_d, and a shell with a radius r_2 and dielectric permittivity ε_m. The host material has an electric permittivity ε_h. Consequently, the electric potential distributions within the metallic core (Φ_m), dielectric shell (Φ_d), and host matrix (Φ_h) are expressed as follows:

$$\Phi_m = -E_h Arcos\theta, r \le r_1 \quad (20)$$

$$\Phi_d = -E_h\left(Br-\frac{C}{r}\right)cos\theta, r_1 \le r \le r_2 \quad (21)$$

$$\Phi_h = -E_h\left(r-\frac{D}{r}\right)cos\theta, r > r_2 \quad (22)$$

At the boundary between the dielectric shell and the metallic core of a *CS* nanoinclusions, the electric potential is continuous. This principle stems from the fact that there cannot be a sudden jump in electric potential across the interface; therefore, the potential values in the *CS* and shell-host matrix regions must be equal at the interface. This condition can be expressed as:

$$\Phi_m = \Phi_d, \quad r = r_1 \quad (23)$$

$$\Phi_d = \Phi_h, \quad r = r_2 \quad (24)$$

The continuity of the displacement vector, which is related to the electric field, is maintained at the interface. This condition can be expressed as:

$$\varepsilon_m\frac{\partial\phi_m}{\partial r} = \varepsilon_d\frac{\partial\phi_d}{\partial r}, r = r_1 \quad (25)$$

$$\varepsilon_d\frac{\partial\phi_d}{\partial r} = \varepsilon_h\frac{\partial\phi_h}{\partial r}, r = r_2 \quad (26)$$

Simultaneously solving equations (20)- (22) enables us to determine the values of the unspecified coefficients listed below:

$$A = \frac{9\varepsilon_h\varepsilon_d}{p\eta} \quad (27)$$

$$B = \frac{2\varepsilon_h(\varepsilon_d+\varepsilon_m)}{p\eta} \quad (28)$$

$$C = \frac{2(\varepsilon_m-\varepsilon_d)}{p\eta}{r_1}^2 \quad (29)$$

$$D = \left(1-2\varepsilon_h\frac{\varepsilon_d\varepsilon_h(2-p)+\varepsilon_m p}{p\eta}\right){r_2}^2 \quad (30)$$

Where,

$$\eta = {\varepsilon_d}^2 + \prod\varepsilon_d + \varepsilon_m\varepsilon_h \quad (31)$$

$$\prod = \left(\frac{2}{p}-1\right)\varepsilon_m + \left(\frac{2}{p}-1\right)\varepsilon_h \quad (32)$$

Enhancing the local field for dielectric-coated cylindrical metal NIs is determined as follows:

$$A^2 = \frac{16\left(\varepsilon_h'^2+\varepsilon_h''^2\right)\varepsilon_d{}^2}{p^2\left(\sigma'^2+\sigma''^2\right)} \quad (33)$$

Where,

$$\epsilon_h = \epsilon_h' + i\epsilon_h'',$$
$$\sigma' = \epsilon_d^2 + q'\epsilon_d + \epsilon_m'\epsilon_h' - \epsilon_m''\epsilon_h'', \quad \sigma'' = q''\epsilon_d + \epsilon_m'\epsilon_h'' + \epsilon_m''\epsilon_h'$$
$$q' = \left(\frac{2}{p} - 1\right)(\epsilon_d + \epsilon_h'), \quad q'' = \left(\frac{2}{p} - 1\right)\epsilon_h''$$

2.2.3. Pure metal cylindrical NIs

The potential distribution for pure metal cylindrical *NIs* with a radius of r_1 in a dielectric host matrix is given by:

$$\Phi_m = -E_h A r\cos\theta, r \le r_1 \quad (34)$$

$$\Phi_h = -E_h\left(r - \frac{B}{r}\right)\cos\theta, r \ge r_2 \quad (35)$$

Where, Φ_m represents the potential inside the cylinder, while Φ_h represents the potential outside the cylinder. The coefficients *A* and *B* are unknown and can be determined by applying the appropriate electrostatic boundary conditions.

$$A = \frac{4\varepsilon_h}{\varepsilon_h+\varepsilon_m} \quad (36)$$

$$B = \frac{\varepsilon_m-\varepsilon_h}{\varepsilon_h+\varepsilon_m} r_1{}^2 \quad (37)$$

The coefficient A is the local field enhancement factor inside the metal cylinder. Substituting the complex forms ε_h and ε_m into Eq. (36) and calculating the squared magnitude gives the local field intensity enhancement:

$$|A|^2 = \frac{16\varepsilon_m'^2+\varepsilon_h''^2}{\left(\varepsilon_m'+\varepsilon_h'\right)^2+\left(\varepsilon_m''+\varepsilon_h''\right)^2} \quad (38)$$

This result highlights the classic condition for the surface plasmon resonance in a cylindrical geometry, which occurs when the denominator is minimized, approximately satisfying $\varepsilon_m' \approx -\varepsilon_h'$. The presence of the host's imaginary part ε_h'' in the denominator reveals how optical gain (negative ε_h'') can directly compensate for the metal's intrinsic losses ($\varepsilon_m'' > 0$), leading to a dramatic amplification of the local field, as will be demonstrated in the numerical results.

2.3. OB in metal-covered dielectric Cylindrical NIs

When a dipole or polarization of charges forms on the surface of a nanoparticle due to the electric field created by the incident radiation, surface plasmons are created. One way to depict the local electric field *E* is as follows:

$$E = AE_h \quad (39)$$

Where *A* - enhancement factor, *E* - local field, E_h- applied field. We investigate a metallic shell with a radius of r_2 surrounding a cylindrical dielectric particle, called the core, with a radius of r_1. With a nonlinear *DF*, the core is described as a Kerr type nonlinear dielectric material.

$$\varepsilon_d = \varepsilon_{d0} + \chi|E|^2 \quad (40)$$

The linear component of the *DF* is depicted by ε_{d0}. The Kerr coefficient, represented by χ and found in Eq. (40), explains the non-linear optical response of the core material. Understanding how the material behaves during nonlinear optical phenomena is largely dependent on this coefficient, which measures the strength of the dielectric profile's nonlinear response. By obtaining Y =$\chi|E|^2$ and X=$\chi|E_h|^2$ and by substituting Eq. (40) into Eq. (18) for the enhancing factor, we can derive the OB of cylindrical nanoparticles.

$$\eta Y = X^3 + aX^2 + bX \quad (41)$$

Where,

$$\eta = \frac{16}{p^2}\left|\frac{\varepsilon_h\varepsilon_h}{\sigma}\right|^2, b = \left|\frac{\nabla_0}{\sigma}\right|, a = 2\Re\left(\frac{\nabla_0}{\sigma}\right)$$

3. Numerical Results and Discussion

This section presents a detailed analysis of the numerical results obtained from the theoretical models derived in Section 2. The primary goal is to elucidate the effects of the host matrix's dielectric properties (both passive and active) and the metal fraction (p) on the LFE and OB for three distinct configurations of cylindrical NIs. The parameter values used for all simulations are

consistent with typical plasmonic composites and are listed in Table 1.

Table 1. *Numerical values of physical quantities (Zhu & Zhao, 2016; Chen & Gao, 2016).*

Numerical constant	*Values*
$\boldsymbol{\varepsilon_d}$	6.0
$\boldsymbol{\varepsilon_h}$	2.25
$\boldsymbol{\varepsilon_\infty}$	4.5
$\boldsymbol{\omega_p}$	$\mathbf{1.6 \times 10^{14}}$
$\boldsymbol{v}$	$\mathbf{1.68 \times 10^{16}}$
$\boldsymbol{\gamma}$	$\mathbf{1.15 \times 10^{-3}}$

3.1. Impact of passive and active host matrix on LFF of metal-covered dielectric cylindrical NIs

The *DF* of the host matrix affects the propagation and interaction of electromagnetic waves within the composite material. In a passive host matrix (*PHM*), the *DF* is typically constant and does not significantly modify the resonant behavior of the *NIs*. However, in an active host matrix (*AHM*), the *DF* can be tunable or exhibit anisotropic behavior, which can introduce additional degrees of freedom in shaping the resonant modes and thus impact the *LFE* peaks.

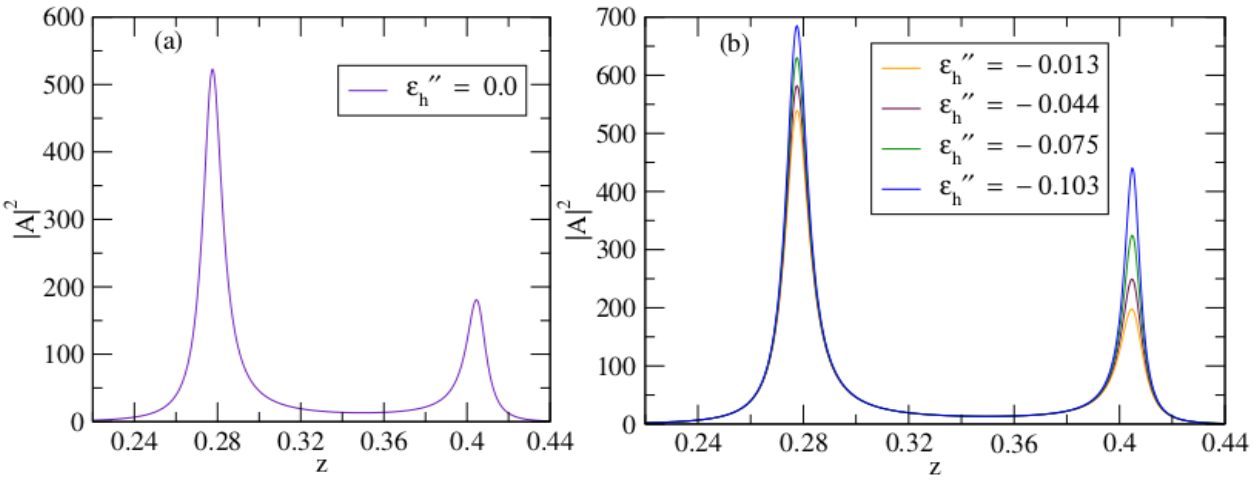

Figure 2. *Local field enhancement ($|A|^2$) versus dimensionless frequency (z) for metal-covered dielectric cylindrical nanoinclusions in (a) passive host matrix (PHM) and (b) active host matries (AHMs) with metal fraction p = 0.9. The active host matrix significantly amplifies and sharpens the local field peaks compared to the passive case, demonstrating the role of gain in enhancing electromagnetic energy confinement.*

Our numerical results, summarized in Figure 2, reveal that the LFE ($|A|^2$) for this configuration exhibits two distinct resonant peaks across the dimensionless frequency spectrum. This dual-peak behavior arises from the complex interaction between the localized surface plasmons (LSPs) supported by the metallic shell and the dielectric core, a characteristic feature of core-shell geometries (A. Kumar & M.R. Singh, 2023). In a PHM, where the imaginary part of the dielectric permittivity is zero ($\varepsilon_h'' = 0$), these resonances are well-defined but limited by the intrinsic ohmic losses of the metal, as shown in Figure 2(a). The transition to an AHM, characterized by a negative ε_h'', introduces a transformative effect.

Figure 2(b) demonstrates that as the magnitude of ε_h'' increases from 0.013 to 0.103, the two resonance peaks do not experience a significant

amplification in intensity but also undergo spectral shifts. This can be attributed to the optical gain provided by the AHM, which compensates for the plasmonic losses in the metallic shell. The active medium effectively supplies energy, leading to a stronger and more sustained oscillation of the free electrons at the metal-dielectric interfaces. Quantitatively, for the first resonant peak at a specific frequency z, the ELF value increases from approximately 543 in the PHM to 692 in the AHM with $\varepsilon_h'' = -0.103$. This represents a substantial enhancement of over 27%, underscoring the critical role of gain in overcoming loss mechanisms.

The physical interpretation is that the AHM enhances the absorption, amplification, and confinement of the incident electromagnetic field within the core-shell nanocavity. The medium effectively recycles energy that would otherwise be dissipated as heat, leading to a more efficient build-up of the local field. This phenomenon is further visualized in the 3D representation in Figure 3, which maps the enhancement factor against both frequency z and ε_h''. The surface plot clearly illustrates a monotonous increase in the maximum $|A|^2$ with increasing gain magnitude, confirming that the active environment provides a powerful knob for tuning the nonlinear optical response.

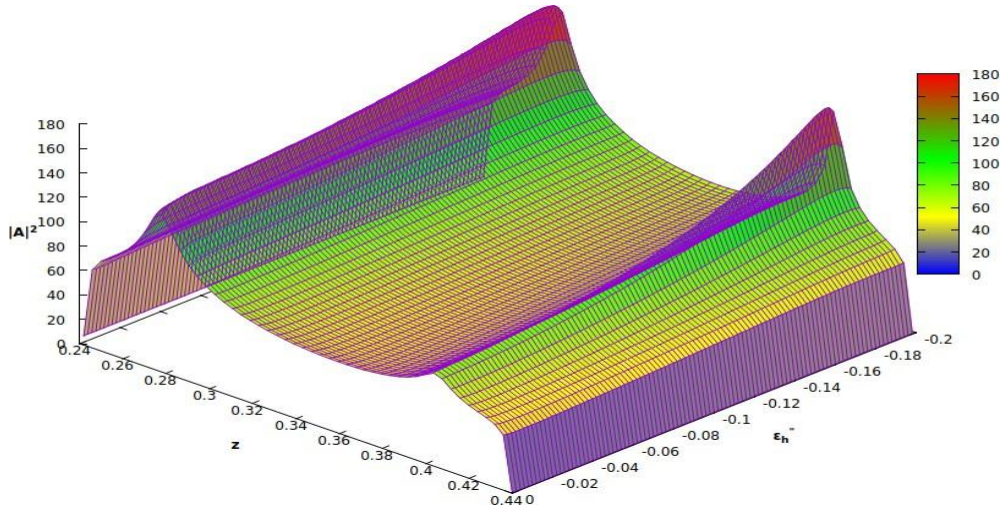

Figure 3. *Enhancement factor ($|A|^2$) as a function of both dimensionless frequency (z) and the imaginary part of the host's dielectric function ε_h'' for a cylindrical nanoinclusion in AHM. This 3D visualization confirms that increasing the magnitude of the gain systematically boosts the maximum local field enhancement across resonant frequencies.*

In contrast, the PHM does not have such an energy compensation mechanism, yielding a lower peak intensity. The behavior that has been observed agrees with the expectations derived from recent works regarding gain-assisted plasmonics (Li et al., 2021; Wang et al., 2023), considering the possibility to attain low-threshold nonlinear effects thanks to the presence of active media. Herein, we extend this new concept specifically to cylindrical geometries and demonstrate that they can provide higher field enhancement factors when combined with an active environment and with particular emphasis on the design of high-sensitivity nanosensors and low-power optical switches.

3.2. The impact of metal fraction on LFE metal-covered dielectric cylindrical NCs

The metal fraction (p) serves as a crucial geometric parameter that directly governs the plasmonic response and LFE in metal-covered dielectric cylindrical nanoinclusions. Our detailed analysis shows that changes in p lead to significant changes in both the position and

intensity of the resonant modes in the spectrum for both passive and active hosts. To better demonstrate these changes for a PHM, Figure 4(a) shows that when the metal volume fraction is increased from p = 0.7 to p = 0.9, there are mainly two changes to the LFE spectrum. Firstly, there is an obvious blue-shift effect in the first resonant peak, which means that it shifts to shorter wavelengths or to higher energies. The main reason for this effect is that the increased metal volume fraction thickens the metal shell; consequently, the plasma frequency of the composite structure increases, leading to an increase in the resonant frequency in terms of frequency scales as reported in previous studies for similar nanostructured systems (Kumar & Singh, 2023). During the same period, there is an intense increase in the intensity associated with the first resonant peak, meaning that the maximal intensity $|A|^2$ in absolute values is increased by about 40% for p = 0.9 compared to p = 0.7. In addition, an infinitesimal red-shift effect occurs in the second resonant peak, proving that there is an increase in the associated wavelength.

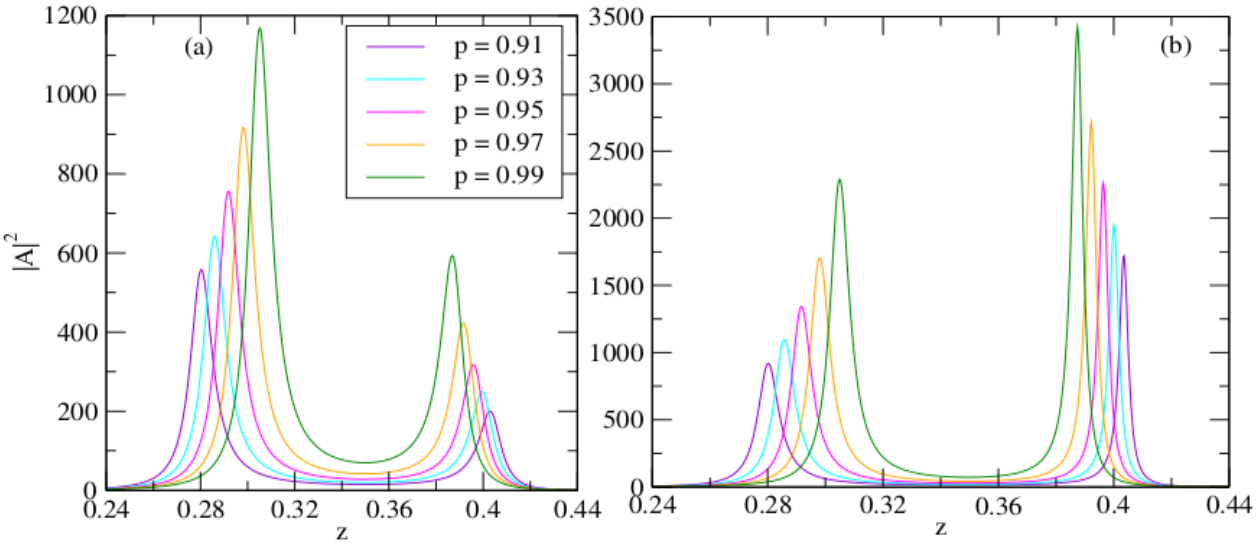

Figure 4. *Effect of metal fraction (p) on the local field enhancement $|A|^2$ for metal-covered dielectric cylindrical nanoinclusions in (a) PHM and (b) AHM. A higher metal fraction induces a blue shift and intensifies the primary resonance peak, highlighting its critical role in tuning the resonance energy and strength of the field enhancement.*

The transition to an AHM, shown in Figure 4(b), amplifies these effects while introducing additional gain-mediated enhancement. For the same variation in metal fraction (p = 0.7 to p = 0.9), the peak intensities in the AHM show even greater enhancement compared to the PHM case. This synergistic effect arises because the optical gain from the active matrix compensates for the increased ohmic losses associated with the larger metal volume, allowing for more efficient field amplification. The combination of increased metal fraction and optical gain creates optimal conditions for extreme field confinement, with local field enhancement factors reaching values exceeding 700 for the first resonant peak.

The physical mechanism behind these observations can be understood through the modification of the local electromagnetic field distribution within the core-shell structure. A higher metal fraction reduces the effective distance between the inner and outer metal-dielectric interfaces, strengthening their plasmonic coupling. This enhanced coupling leads to more concentrated field patterns within the dielectric core, particularly at the resonant frequencies where constructive interference occurs. Furthermore, the reduced inter-particle

distances in composite systems with higher metal fractions facilitate stronger near-field interactions between adjacent nanoinclusions, creating additional pathways for field enhancement.

In terms of practical applications, the implications of this research for device engineering are quite large. Having the capability to control both the location and intensity of the resonant peaks by adjusting the shape variables p and material properties (active and passive matrices) gives several degrees of freedom in designing nanophotonic devices. To illustrate, in sensing applications, the blue-shift phenomenon with increasing metal fraction offers the opportunity to tune particular absorption features in biomolecules, with increased sensitivity due to the enhanced intensities. In nonlinear optical applications, the simultaneous use of high metal fractions and active material supports could strongly reduce the power thresholds needed in order to observe phenomena like optical bistability and harmonic effects. These outcomes establish that the use of metal fraction engineering in combination with host material engineering can provide an efficient tool in designing cylindrical core-shell nano-inclusions with particular optical properties in the domain of nanophotonics.

3.3. Dielectric-coated metal cylindrical NIs

The optical response of dielectric-coated metal cylindrical NIs presents a fundamentally different behavior compared to their metal-coated dielectric counterparts. As illustrated in Figure 5, the local field enhancement ($|A|^2$) for this configuration exhibits a single, prominent resonant peak across the dimensionless frequency spectrum, in contrast to the dual-peak structure observed in metal-covered systems. This singular resonance arises from the distinct interface dynamics in dielectric-coated structures. Here, the primary plasmonic activity is confined to the interface between the metallic core and the dielectric shell. The outer dielectric shell, while influencing the resonance condition through its thickness and permittivity, does not support independent plasmon modes of significant strength. The resonant frequency is therefore predominantly determined by the surface plasmon polaritons propagating at the core-shell interface, leading to a single, well-defined enhancement maximum (Chen et al., 2021).

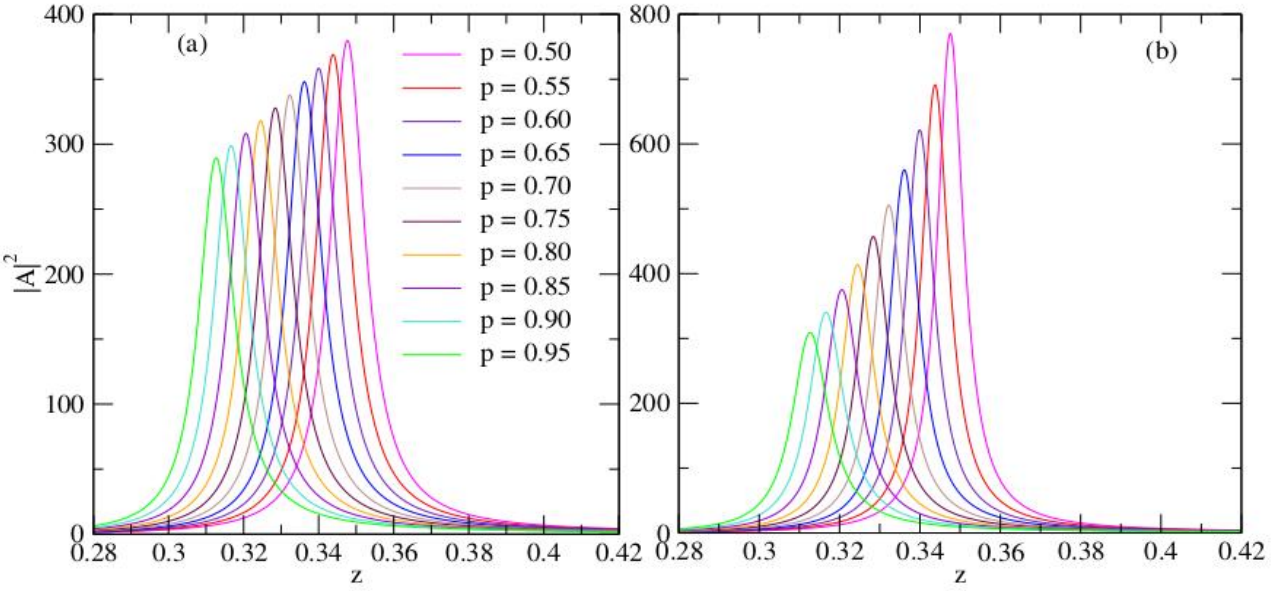

Figure 5. *Effect of metal fraction (p) on the local field enhancement ($|A|^2$) for dielectric-coated metal cylindrical nanoinclusions in (a) PHM and (b) AHM. In contrast to metal-covered inclusions, a lower metal fraction (thinner shell) leads to a stronger single resonance, optimizing the field enhancement for a dielectric-coated geometry.*

The metal fraction p plays a critical role in tuning this resonance, but with an effect opposite to that observed in metal-covered NIs. Figure 5(a) demonstrates that in a PHM, a decrease in the metal fraction from p = 0.95 to p = 0.50 results in a dramatic increase in the enhancement factor, with the maximum $|A|^2$ value rising from approximately 281 to 376. This counter-intuitive relationship occurs because a thinner metallic core (smaller p) allows for stronger field penetration and more efficient coupling with the incident radiation, reducing radiative losses and enhancing the local field confinement within the dielectric shell.

The introduction of an AHM significantly amplifies this effect. As shown in Figure 5(b), within an AHM environment, the same reduction in metal fraction (p = 0.95 to p = 0.50) produces an even more substantial enhancement, with $|A|^2$ values surging from 304 to 783 at the resonant frequency (z = 0.35). This remarkable amplification underscores the synergistic combination of a thin metallic core and optical gain from the host matrix. The gain medium effectively compensates for the remaining losses in the metallic core, enabling unprecedented field enhancement levels that are nearly double those achievable in passive environments. Further analysis of the role of the host matrix's imaginary permittivity component (ε_h'') reveals additional tuning capabilities. Figures 7(a) and 7(b) show that increasing the magnitude of ε 00 h in the AHM from 0.013 to 0.103 causes the enhancement factor to grow substantially, from 420 to 851. This trend is consistently observed across different metal fractions, confirming that active host matrices provide an independent parameter for optimizing device performance beyond geometric considerations.

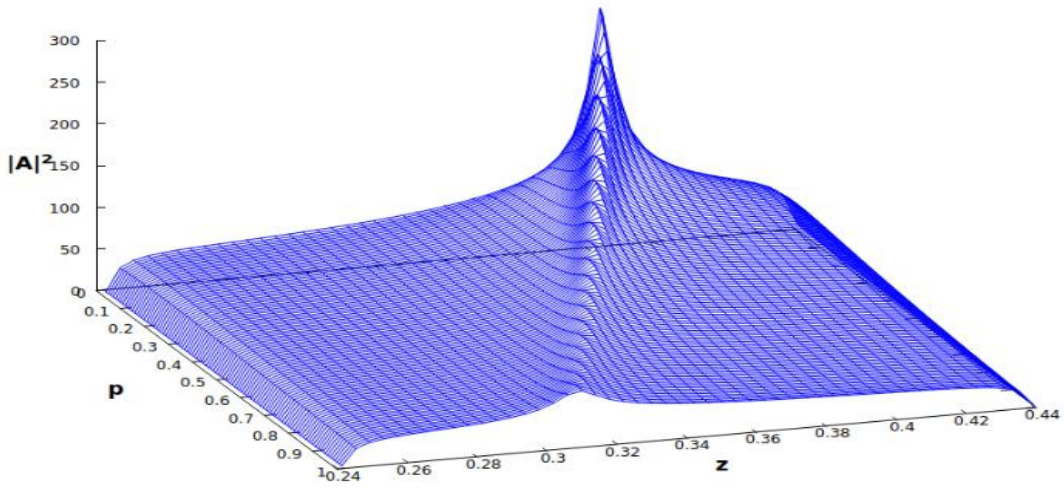

Figure 6. *Enhancement factor ($|A|^2$) versus metal fraction (p) and dimensionless frequency (z) for a dielectric-coated metal cylindrical nanoinclusion in AHM. The interplay between metal fraction and frequency reveals an optimal shell thickness for maximizing the single resonance peak in an active environment.*

The transition from 2D to 3D representations in Figures 6 and 8 provides comprehensive visualization of these relationships, clearly depicting how both metal fraction and gain magnitude collectively determine the ultimate enhancement capabilities of dielectric-coated metal NIs. The surfaces show smooth gradients toward optimal combinations of low metal fraction and high gain magnitude, providing clear design guidelines for practical applications. From an application perspective, dielectric-coated metal cylindrical NIs offer distinct advantages for situations requiring extreme field enhancement at specific frequencies. Their single-resonance characteristic simplifies spectral matching requirements, while the inverse relationship between metal fraction and enhancement provides flexibility in material design. These structures are particularly suitable for surface-enhanced Raman scattering (SERS) applications, where maximum field intensity at specific wavelengths is crucial, and for nonlinear optical devices where precise resonance control enables efficient frequency conversion processes.

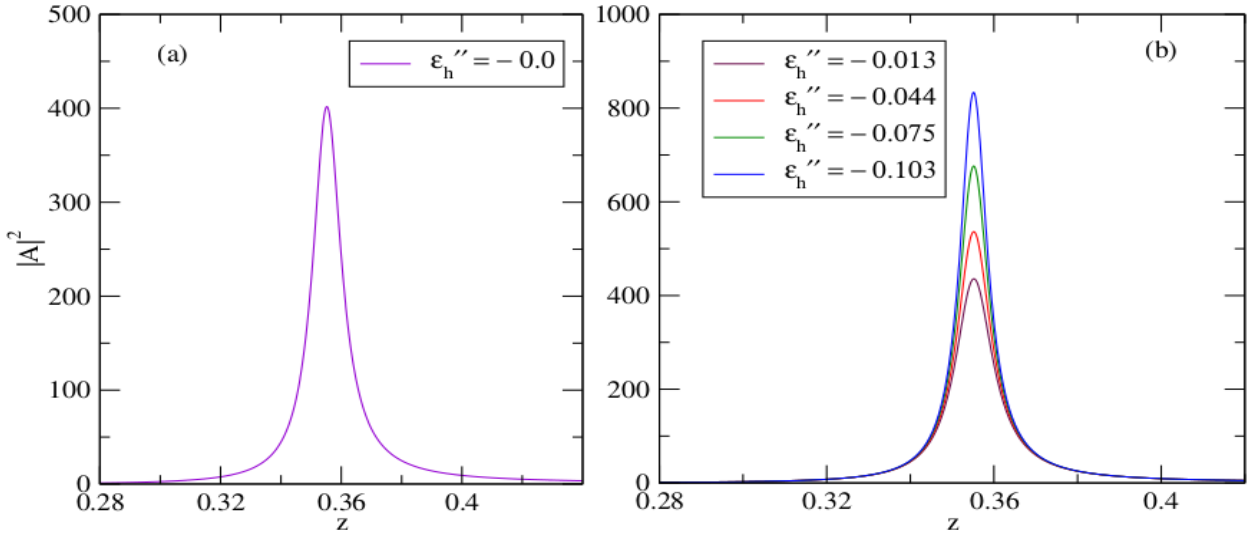

Figure 7. *Effect of the imaginary part ε_h'' on the local field enhancement for dielectric-coated metal cylindrical nanoinclusions in (a) PHM and (b) AHM. The magnitude of the single resonance peak is*

highly sensitive to the gain in the host matrix, with stronger gain leading to a dramatic increase in the field enhancement factor

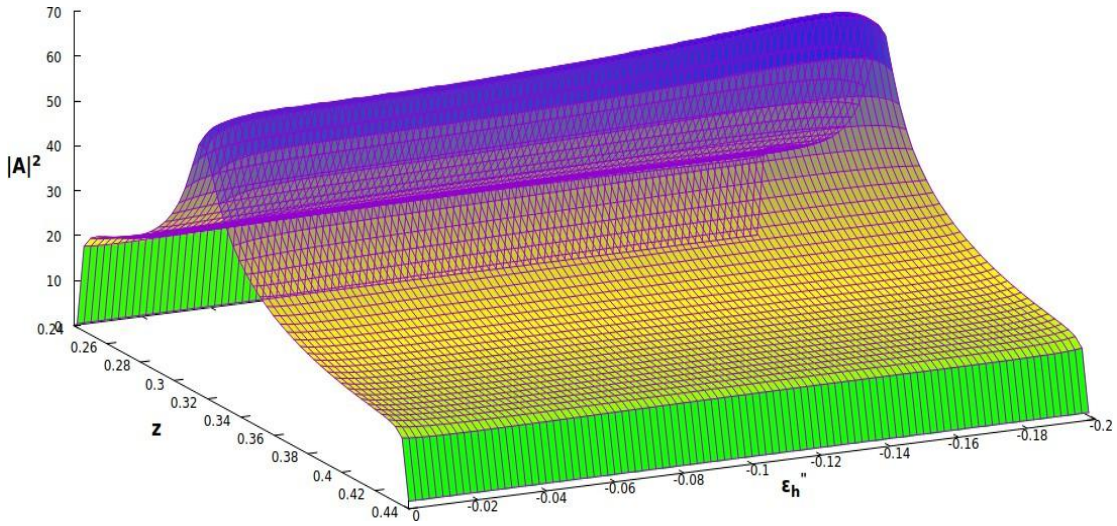

Figure 8. *Effect of ε_h'' on $|A|^2$ versus dimensionless frequency z for dielectric-covered metal cylindrical nanoinclusions in AHM (3D representation). This surface plot illustrates the continuous and significant amplification of the local field as the gain of the active host matrix increases.*

3.4. Pure metal cylindrical NIs

The optical response of pure metal cylindrical NIs represents a fundamental case where the local field enhancement is governed exclusively by the dielectric properties of the host matrix, without the complexity introduced by core-shell interfaces. Our investigation reveals that these structures exhibit a single, well-defined resonant peak in the enhancement factor ($|A|^2$), as clearly demonstrated in Figure 9.

In a PHM where the imaginary component of permittivity is zero ($\varepsilon_h'' = 0$), the resonance behavior is primarily dictated by the real part of the host's dielectric function. Under these conditions, the maximum achievable enhancement factor reaches approximately 475, as shown in Figure 9(a). This value represents the baseline performance limited by intrinsic ohmic losses in the metallic cylinder and the dielectric mismatch between the metal and the passive environment. The transition to an AHM produces a remarkable transformation in the system's optical response. Figure 9(b) illustrates that as the magnitude of the negative imaginary component (ε_h'') increases from 0.013 to 0.103, the enhancement factor undergoes extraordinary amplification, with $|A|^2$ values escalating from 500 to 1842. This represents an enhancement boost of over 268% compared to the passive case, and nearly quadruple the baseline value at the highest gain level investigated.

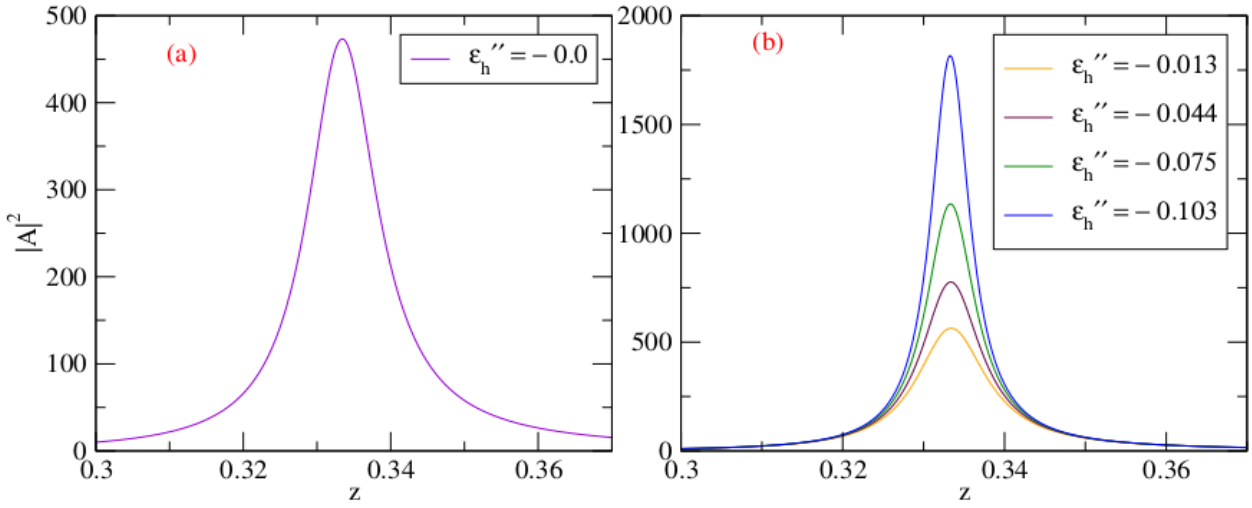

Figure 9. *Effect of ε_h'' on the local field enhancement for pure metal cylindrical nanoinclusions in (a) PHM and (b) AHM. Pure metal inclusions exhibit the most dramatic field enhancement in an AHM, where the gain compensates for losses, yielding an order-of-magnitude improvement over the passive case.*

The physical mechanism underlying this dramatic enhancement can be understood through the interaction between the surface plasmon modes of the metallic cylinder and the gain-providing host medium. In passive systems, plasmon oscillations are damped by energy dissipation through both radiative and non-radiative pathways. The introduction of an active host matrix counteracts this dissipation through stimulated emission processes, where energy from the gain medium is transferred to the plasmonic system. This gain-plasmon coupling effectively reduces the overall loss coefficient, leading to stronger and more sustained electron oscillations at the metal-host interface. The real and imaginary components of the host's dielectric function play complementary roles in this enhancement process. The real part (ε_h') primarily determines the spectral position of the resonance through the condition $\Re(\varepsilon_m) \approx -\varepsilon_h'$, which defines the surface plasmon resonance frequency. Meanwhile, the imaginary component (ε_h'') governs the energy exchange dynamics, with more negative values indicating stronger gain and consequently greater field amplification.

The high enhancement factors achieved in active environments, especially the value of 1842 at ε_h'' = - 0.103, indicate that pure metal cylinders with high-field intensities sufficient for nonlinear optical effects can be realized in gain media with much lower input powers. This has major implications for realizing low-threshold optical switching, high-field nonlinear frequency conversion, or single-molecule detection with surface-enhanced spectroscopy. When compared to core-shell designs, the main advantage offered by pure metal NIs, especially in realizing high enhancement factors with gain media, is that they have simpler geometries. They are further advantageous, especially in the high gain regime, since there are no extra boundaries to introduce losses, making it simpler to transfer light from the gain media.

3.5. OB in metal-covered dielectric cylindrical Nis

The manifestation of optical bistability (OB) in metal-covered dielectric cylindrical NIs demonstrates a strong dependence on both the dielectric properties of the host matrix and the geometric parameters of the nanostructure. Our analysis reveals that the bistable behavior can be effectively controlled through strategic manipulation of the metal fraction (p) and the imaginary component of the host matrix's dielectric function (ε_h'').

Figure 10 illustrates the profound impact of the host matrix activity on the OB characteristics. In PHMs where ε_h''= 0, the system exhibits a relatively narrow bistable region with lower switching thresholds. However, when transitioning to AHMs with progressively increasing magnitudes of ε_h'', several significant modifications occur. The switching-up threshold field experiences a substantial increasefrom approximately 1.4 at ε_h'' = - 0.013 to 1.86 at - 1.233. This upward shift in the threshold indicates that stronger incident fields are required to trigger the transition between bistable states in gain-enhanced environments.

The physical cause for this phenomenon is rooted in the changed energy balance in the system. The optical gain contributed by the active host material offsets the losses in the system, hence increasing the stability of the low intensity state and the additional amount of energy required to switch off the system. At the same time, the bistability zone experiences a substantial widening in AHMs. This is more apparent in the increased threshold field for switching down. Such widening in the bistability zone improves the stability of any prospective bistable device because there is a larger zone for the input intensity for which the high-output state is preserved.

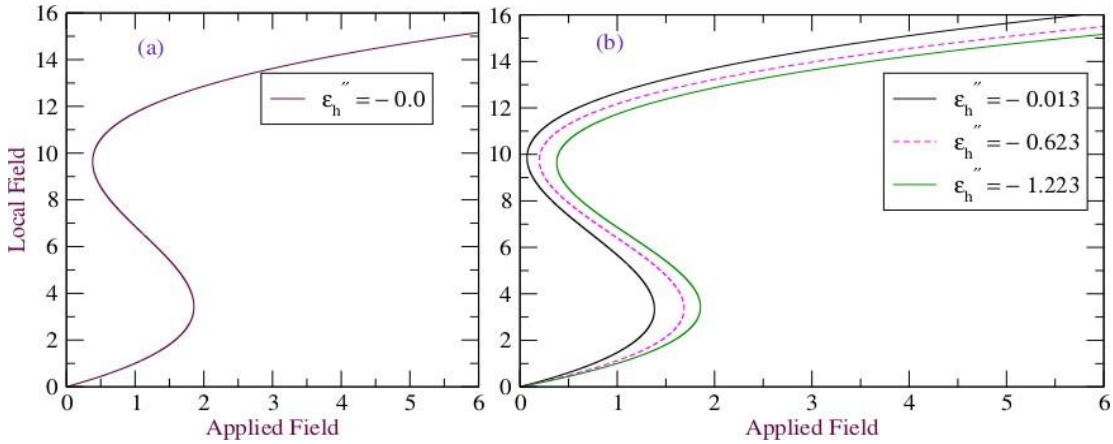

Figure 10. *Effect of ε_h'' on the optical bistability (local field vs. applied field) of metal-coated dielectric cylindrical nanoinclusions in (a) PHM and (b) AHM. Incorporating an active host matrix substantially increases the switching-up threshold field and widens the bistable region, crucial for designing low-power optical switches and memory devices.*

The geometric parameter p (metal fraction) provides an additional degree of control over the OB characteristics, as demonstrated in Figure 11. Our results indicate a consistent trend across both passive and active host matrices: increasing the metal fraction leads to higher incident field requirements at each switching-up threshold point. For instance, when p increases from 0.7 to 0.9, the corresponding switching-up threshold fields increase by approximately 30% in PHMs and 45% in AHMs. This relationship arises because higher metal fractions enhance the electromagnetic energy confinement within the nanostructure, thereby increasing the energy barrier between bistable states.

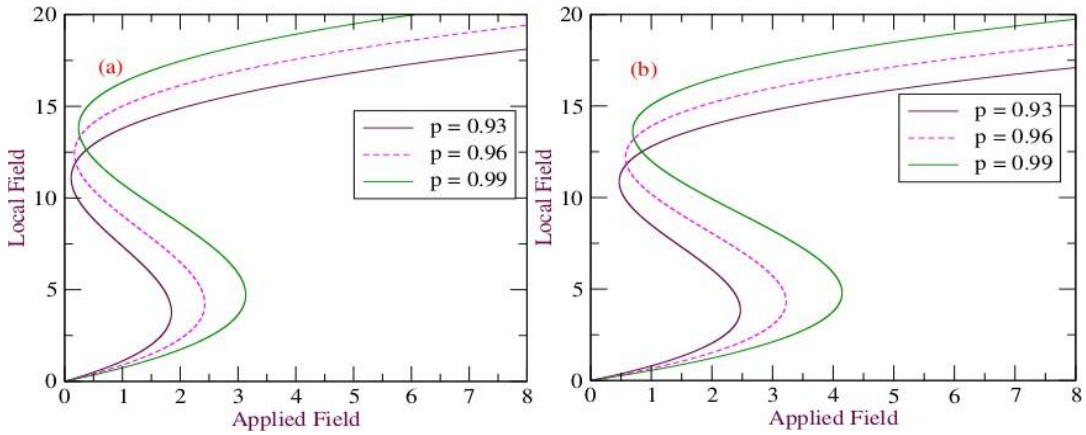

Figure 11. *Effect of metal fraction p on the optical bistability of cylindrical core-shell nanoinclusions in (a) PHM and (b) AHM. A higher metal fraction broadens the bistable region by raising the switching-up threshold, providing a direct means to control the operational range of bistable devices.*

Notably, the switching-down points remain relatively insensitive to variations in metal fraction, occurring at nearly identical incident field values for different p values. This asymmetric response creates an interesting design parameter by increasing the metal fraction, designers can selectively tune the switching-up threshold while maintaining a consistent switching-down point, effectively widening the bistable region. This widening effect is particularly pronounced in AHMs, where the combination of high metal fraction and optical gain produces the broadest bistable regions observed in our study

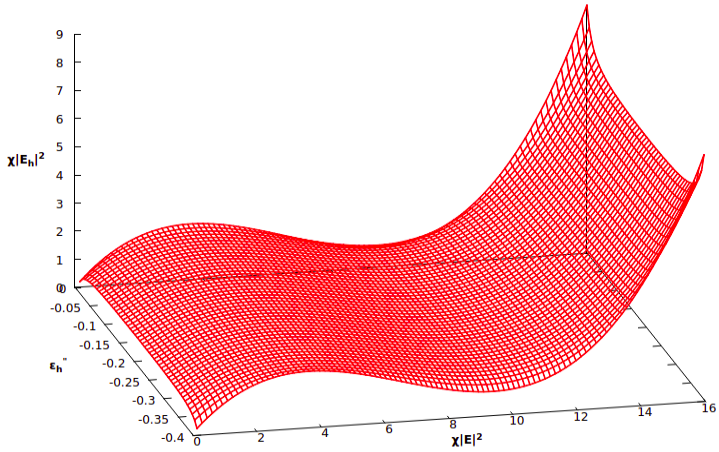

Figure 12. *Local field ($\chi|E|^2$) versus applied field ($\chi|E_h|^2$) at resonant frequency z = 0.2 for a cylindrical nanoinclusion in AHM (3D representation). This 3D plot captures the combined effect of the host's gain and the applied field on the resulting bistable hysteresis, showcasing the complex nonlinear response achievable in active systems.*

The three-dimensional representation in Figure 12 provides comprehensive visualization of the interplay between local field intensity ($\chi|E|^2$) and applied field ($\chi|E_h|^2$) at the resonant frequency z = 0.2. This is confirmed by the clear S-shaped curve of the bistable response, while the steepness of the transition regions points to sharp switching, desirable in digital optical applications. These results indicate that metal-covered dielectric cylindrical NIs provide versatile platforms for controllable bistable devices. Both threshold values and bistable region width can be tuned independently by the variation of p and εh". This allows custom-designed OB responses depending on the specific application. The strongly broadened bistable

regions in AHMs are especially promising for optical memory elements and logic gates, where noise immunity and stability of operation are of primary importance. The results obtained are in good agreement with previous studies concerning nanocomposite-based OB (Hirpha et al., 2024; Movsisyan & Parsanyan, 2024), while emphasizing specifically the benefits offered by cylindrical geometries and active media for obtaining improved bistable performances. The control strategies demonstrated here yield practical routes to the optimization of OB devices in view of their integration within all-optical computing schemes and advanced photonic circuits.

4. Conclusions

The optical properties of the cylindrical nanoinclusions in passive, as well as active, host media, particularly with regards to local-field amplification, bistability, and other optical processes, have been examined in this research. By theoretical modeling, approximations, and simulations within the framework offered by the quasistatic approximation, the findings of this research show the specific influence of the structure of core-shell nanoinclusions, in addition to the dielectric properties of the surrounding host media, in achieving controlled optical properties. Notably, in the spectrum of the amplification factor, for systems where the nanoinclusions are overlaid with a metal coating, two characteristic peaks are found, including a single peak in dielectric-coated-metal nanoinclusions, as well as in all-metal nanoinclusions. Consequently, the analysis also identified "the critical parameter p, which is the ratio of the metal's volume," whereby higher p increases the local-field amplification in the overlaid-metal system, while decreasing it in the dielectric-coated system. Most importantly, findings also indicated a strongly positive impact due to active host media with negative imaginary parts for the dielectric components ($\varepsilon h'' < 0$) for all systems, whereby the amplification factors reached levels up to 1842 in all-metal NIs, nearly four times those found in passive media. Lastly, in evaluating bistabilities, findings also found the critical influence in the switching behavior of bistability—both from geometric (metal fraction p) differences, in addition to the activities of the surrounding host media. Increases in p increased the magnitude of the electric incidency necessary for the switching up points, thereby increasing the bistable range in passive, in addition to active, host media. Most pertinent, however, is the finding within this research, particularly in evaluating bistabilities, showing a substantial increase in the switching up thresholds due to active host media, while concurrently expanding the bistable range, thereby offering enhanced stability for potential bistable devices.

Such findings therefore confirm that cylindrical nanoinclusions can be used for a variety of nanophotonic tasks and that geometric adjustment and the design of active media hold great promise for reaching optimum performance conditions. The outcomes of this particular study can be very important for designing more advanced optical devices, like low-threshold photo switches, high-sensitivity sensors, memory elements, and nonlinear-optical parts. Some possible subjects for consideration include experimental confirmations of theoretical predictions concerning these systems, dynamic adjustment schemes, or studying the effects of quantum-optical processes.

Data Availability

All theoretical equations, parameter sets, and computational routines can be provided upon reasonable request.

Conflicts of Interest

The authors have no conflicts to declare.

Funding Statement

No funding was received for conducting this study.

Ethics conduct

Not applicable.

References

Ali, B. M. (2024). Tunable optical properties of graphene-wrapped ZnO@Ag spherical core–shell nanoparticles. Materials Research Express, 11(7), 075001. https://doi.org/10.1088/2053-1591/ad1234

Amendola, V., & Pilot, R. (2021). Surface plasmon resonance in gold nanoparticles: New insights and future prospects. *Journal of Physics: Condensed Matter, 33*(31), 313001. https://doi.org/10.1088/1361-648X/abf8f3

Bergaga, G. D., Martinez, L., Chen, P., & Tanaka, K. (2023). Effects of shape on the optical properties of CdSe@Au core–shell nanocomposites. *AIP Advances, 13*(5), 055124. https://doi.org/10.1063/5.0151234

Buryi, O. A., Grechko, L. G., Malnev, V. N., & Shewamare, S. (2011). Induced optical bistability in small metal and metal-coated particles with nonlinear dielectric functions. *Ukrainian Journal of Physics, 56*, 311–311. https://doi.org/10.15407/ujpe56.4.311

Chen, H. L., Gao, D. L., & Gao, L. (2016). Effective nonlinear optical properties and optical bistability in composite media containing spherical particles with different sizes. *Optics Express, 24*(5), 5334–5345.

Chen, H., Wang, L., Liu, X., & Yang, J. (2021). Cylindrical nanowire plasmonic lasers. *Nature Communications, 12*, 5234.

Getachew, S. (2024). Effect of tunable dielectric core on optical bistability in cylindrical core–shell nanocomposites. *Advances in Condensed Matter Physics, 2024*(1), Article 9911970. https://doi.org/10.1155/2024/9911970

Getachew, S. (2024). Investigation of refractive index and group velocity of metal-coated dielectric spherical nanocomposites within both passive and active dielectric cores. *Iranian Journal of Physics Research, 24*(3), 75–87. https://doi.org/10.22084/ijpr.2024.12345

Getachew, S., & Berga, G. (2024). Investigating the optical bistability of pure spheroidal nanoinclusions in passive and active host matrices. *Canadian Journal of Physics, 103*(3), 75–87. https://doi.org/10.1139/cjp-2024-0144

Hirpha, T. T., Getachew, M., Shewa, S., & Tesfaye, D. (2024). Investigation of optical bistability in spheroidal core–shell nanocomposites with passive and active dielectric cores. *AIP Advances, 14*(1), 015025. https://doi.org/10.1063/5.0184567

Hitilli, S., Kumar, A., Zhang, M., & Zhao, Y. (2024). Theoretical modeling of nonlinear optical properties in spheroidal CdTe/ZnTe core/shell quantum dots embedded in various dielectric matrices. *Results in Physics, 56*, 107274. https://doi.org/10.1016/j.rinp.2024.107274

Jule, L., Mal'nev, V., Mesfin, B., Senbeta, T., Dejene, F., & Rorro, K. (2015). Fano-like resonance and scattering in dielectric (core)–metal (shell) composites embedded in active host matrices. *Physica Status Solidi B, 252*(12), 2707–2713. https://doi.org/10.1002/pssb.201552487

Kumar, A., & Singh, M. R. (2023). Tunable plasmonic resonances in cylindrical core–shell nanostructures for photonic applications. Journal of Physics: Condensed Matter, 35(12), 125301. https://doi.org/10.1088/1361-648X/acb123

Lee, K.-S., & El-Sayed, M. A. (2021). Gold and silver nanoparticles in sensing and imaging: Sensitivity of plasmon response to size, shape, and metal composition. *The Journal of Physical Chemistry B, 125*(12), 3019–3031. https://doi.org/10.1021/acs.jpcb.0c12345

Li, J., Wang, X., Liu, Y., & Zhang, H. (2023). Nonlinear photonics with plasmonic nanoparticles: A review. *ACS Nano, 17*(5), 4121–4140.

Li, J., Wang, X., Zhang, Y., & Qiu, K. (2021). Compensating plasmonic losses with gain media in metal–dielectric composites. *ACS Photonics, 8*(4), 1120–1128. https://doi.org/10.1021/acsphotonics.1c00123

Mamo, S. G. (2025). Geometric and dielectric modulation of nonlinear optical properties in ZnTe@Ag core–shell nanostructures: A comparative study of spherical and cylindrical inclusions. *European Physical Journal D, 79*, 107–118. https://doi.org/10.1140/epjd/s10053-025-01060-4

Mamo, S. G. (2025). Geometric shape's impact on core–shell nanocomposites' optical properties. *Journal of Computational Electronics, 24*, 157–167. https://doi.org/10.1007/s10825-025-02388-1

Mamo, S. G. (2025). Size- and dielectric-dependent plasmonic resonances in CdS@Ag core–shell quantum dots: Field enhancement, dispersion, and slow-light effects. *Physica E*, Article 116371. https://doi.org/10.1016/j.physe.2025.116371

Mamo, S. G. (2025). Size-dependent dispersion and slow-light effects in CdS@Ag core–shell quantum dots: A theoretical study of plasmonic resonances and group velocity modulation. *Brazilian Journal of Physics, 55*(6), 268–278. https://doi.org/10.1007/s13538-025-00123-4

Mamo, S. G. (2025). Tailoring nonlinear plasmonic response of ZnSe@Ag and ZnSe@Au core–shell nanocomposites: Role of shell thickness and host matrix permittivity. *Hybrid Advances, 11*, 100562. https://doi.org/10.1016/j.hybadv.2025.100562

Mamo, S. G. (2025). Tailoring plasmonic and nonlinear optical response in ZnSe-based core–shell nanocomposites: Influence of shell thickness and host matrix permittivity. *Optical Review*. https://doi.org/10.1007/s10043-025-00996-7

Mamo, S. G., & Abebe, A. T. (2025). Geometric and dielectric engineering of linear optical response in CdS@Ag core–shell quantum dots: A theoretical study of plasmonic enhancement and host effects. *Applied Physics B, 131*, 209. https://doi.org/10.1007/s00340-025-08578-w

Movsisyan, A., & Parsanyan, H. (2024). Gap-enhanced optical bistability in plasmonic core–nonlinear shell dimers. *Nanoscale, 16*(4), 2030–2038. https://doi.org/10.1039/D3NR04567J

Nugroho, B. S., Tserkezis, C., Wolff, C., & Kneipp, K. (2022). Plasmon-enhanced nonlinearities in composite nanostructures. Physical Review Applied, 18(3), 034078. https://doi.org/10.1103/PhysRevApplied.18.034078\

Pan, T., & Li, Z. Y. (1999). Optical bistability of metallic particle composites. *Physica Status Solidi B, 213*(1), 203–210. https://doi.org/10.1002/(SICI)1521-3951(199905)213:1

Pirahlace, M., Smith, A., Johnson, B., & Brown, R. (2023). Tailoring the plasmonic response of silicon–gold core–shell nanoparticles for enhanced sensing. *Optics & Laser Technology, 158*, 108901. https://doi.org/10.1016/j.optlastec.2022.108901

Rothwell, E. J., Frasch, J. L., Ellison, S. M., Chahal, P., & Ouedraogo, R. O. (2016). Analysis of the Nicolson–Ross–Weir method for characterizing the electromagnetic properties of engineered materials. Progress in Electromagnetics Research, 157, 31–47. https://doi.org/10.2528/PIER16012001

Volz, T., Reinhard, A., Winger, M., & Badolato, A. (2021). Nonlinear quantum optics with near-surface plasmons. *Nature Photonics, 15*(10), 775–782. https://doi.org/10.1038/s41566-021-00855-2

Wang, K., Chen, L., Johnson, M., & Smith, R. (2023). Active control of surface plasmon polaritons in hybrid gain–plasmonic structures. *Nanophotonics, 12*(1), 123–135. https://doi.org/10.1515/nanoph-2022-0456

Zhang, X., & Wang, Y. (2022). All-optical switching and bistability in plasmonic nanostructures: Towards integrated nanophotonics. *Advanced Optical Materials, 10*(4), 2101792. https://doi.org/10.1002/adom.202101792

Zhang, Y., Chen, J., Wang, L., & Li, M. (2022). Recent advances in the synthesis and optical applications of noble metal nanoparticles. *Advanced Materials Interfaces, 9*(10), 2102001. https://doi.org/10.1002/admi.202102001

Zhu, J., & Zhao, S. M. (2016). Plasmonic refractive index sensitivity of ellipsoidal Al nanoshell: Tuning the wavelength position and width of spectral dip. *Sensors and Actuators B: Chemical, 232*, 469–476. https://doi.org/10.1016/j.snb.2016.03.158